pubs.acs.org/IC

# Redox "Innocence" of Re(I) in Electrochemical CO<sub>2</sub> Reduction Catalyzed by Nanographene-Re Complexes

Richard N. Schaugaard, Krishnan Raghavachari,\* and Liang-shi Li\*

Department of Chemistry, Indiana University, Bloomington, Indiana 47405, United States

Supporting Information

ABSTRACT: Improving energy efficiency of electrocatalytic CO<sub>2</sub> conversion to useful chemicals poses a significant scientific challenge. Recently we reported on using a colloidal nanographene as the diimine ligand to form a molecular complex Re(diimine)(CO)<sub>3</sub>Cl to tackle this challenge, leading to significantly improved CO<sub>2</sub> reduction potential. In this work, we use theoretical computations to investigate the roles of the nanographene ligand in the reduction and the reaction pathways. Remarkably, our results show that the metal center merely provides a binding site for CO<sub>2</sub> and a conduit for electron transfer between the nanographene ligand and the substrate instead of changing its own oxidation state in the processes.

Thus, despite its multiple oxidation states, the Re is redox "innocent" in the CO<sub>2</sub> reduction catalyzed by the nanographene complex.

## ■ INTRODUCTION

The negative environmental impact of the increasing levels of carbon dioxide in the atmosphere can be profound, and mitigating its impact is an important scientific challenge. An important avenue of exploration in this context is the electrochemical or photochemical conversion of CO2 to fuels or other valueadded chemicals using renewable energy sources. 1-9 Despite substantial research efforts on various catalysts to drive such chemical transformations, low energy efficiency is still the major bottleneck preventing their large-scale implementation. Molecular catalysts have the potential to selectively direct chemical reactions along specific multielectron pathways and have attracted substantial interest in this context to achieve high efficiency in conjunction with selectivity. 2,5 However, high overpotentials still plague the catalysts being explored for achieving CO<sub>2</sub> conversion, and new strategies need to be developed to improve their performance. <sup>2,3,10</sup>

Toward this end, we recently introduced nanographenes as a new class of redox noninnocent ligands in metal complexes that, because of their large conjugation size, enable an expanded range of tunability in reduction potentials of the molecular catalysts. For example, complex 1 (Scheme 1) can be readily reduced electrochemically and in the presence of a proton source can achieve the selective conversion of CO<sub>2</sub> to CO with one of the lowest overpotentials reported for molecular catalysts. 11 Our preliminary results have shown that the complex undergoes two one-electron reduction steps to initiate the catalysis, the first being ligand centered and the second delocalized over both the ligand and the metal center. It is the electron delocalization in the second reduction that decreases the reduction potential for the CO<sub>2</sub> reduction.<sup>11</sup> In this study, we provide detailed computational studies of the associated catalytic reaction mechanisms. By studying the electronic coupling between the ligand and the metal center, we show that the Re center, instead of undergoing valence change commonly believed to occur in the related Re(bpy)(CO)<sub>3</sub>Cl system, merely provides a binding site for CO2 and a conduit for electron transfer between the nanographene ligand and the substrate.

### COMPUTATIONAL DETAILS

All calculations were carried out based on unrestricted Kohn-Sham density functional theory (UKS-DFT) with the quantum chemical program package ORCA 3.0.3<sup>12</sup> using the hybrid exchange-correlation functional B3LYP, 13-16 following the work of Carter and co-workers. 17,18 Dispersion interactions were included using Grimme's empirical pairwise D3 corrections<sup>19</sup> in conjunction with the Becke–Johnson damping scheme.<sup>20–22</sup> Geometry optimizations of various chemical species and vibrational mode calculations were done with the def2-SVP basis set.<sup>23</sup> For computational expediency, the core electrons of Re were modeled using the Stuttgart/Dresden effective core potential<sup>24</sup> for that atom. A COSMO (conductor-like screening model)<sup>25</sup> continuum solvation method was used to estimate the free energy of solvation in THF ( $\varepsilon$  = 7.25). Geometry optimizations have been performed on a solvation-corrected potential energy surface (PES) since it has been demonstrated that charge stabilization at the anionic oxygens of activated CO2 is needed to properly model CO2 binding at a reduced metal site in solution. 26 With these calculations we can obtain the free energy term used to

Received: April 19, 2018 Published: August 20, 2018

10548

Scheme 1. Structures of Nanographene-Re Complex (1) We Studied and the Ligand La

<sup>a</sup>L is partitioned and labeled.

construct the PES, that is,  $G_{\rm PES} = E_{\rm SCF} + \Delta G_{\rm COSMO}$ , where  $E_{\rm SCF}$  is the energy calculated with DFT and  $\Delta G_{\rm COSMO}$  is the COSMO solvation correction. Vibrational frequencies were also calculated numerically with COSMO corrections, as it is essential to calculate the Hessian matrices on the same PES as the optimization to obtain meaningful results. No imaginary frequencies were observed for the vibrational modes of the ground-state structures, and only one imaginary frequency was present for transition states.

Accurate energies were obtained by performing single point calculations on the def2-SVP optimized geometries utilizing the maug-def2-TZVPP basis set<sup>27-30</sup> which is augmented with an efficient set of diffuse functions appropriate for a system of this size. Entropy and zero point energy (ZPE) were obtained for polyatomic species from vibrational frequency calculations. For single atom ions, translational entropy was estimated from the Sackur–Tetrode equation by assuming free range of motion in the solution phase, as described by the COSMO protocol. All even electron species were calculated as both singles and triplets with broken symmetry calculations carried out using the high-spin state as a starting point.

The thermally corrected free energy of each species is reported by combining the SCF energy, COSMO solvation energy, ZPE, and the entropic contribution at 298.15 K, that is,  $G_{\rm sol}^0 = E_{\rm SCF} + \Delta G_{\rm COSMO} + {\rm ZPE} - 298.15$  K ×  $S_{\rm total}$ , where  $S = S_{\rm trans} + S_{\rm rot} + S_{\rm vib} + S_{\rm elec}$ . The terms  $S_{\rm trans}$ ,  $S_{\rm rot}$  and  $S_{\rm vib}$  were obtained from the harmonic oscillator and rigid rotor approximations, and  $S_{\rm elec}$  was estimated from the formula  $S_{\rm el} = R \ln(q_{\rm elec})$ , where R is the gas constant and  $q_{\rm elec}$  is the multiplicity of the species. All species were assumed to remain in the solution phase unless released as a gas.

The standard states for the resulting  $G_{sol}^0$  values were gases under a pressure of 1 atm for CO<sub>2</sub> and CO and solution with concentration of 1 M for nongaseous substances unless otherwise stated. Data for the solubility of CO2 at 298.15 K were taken from the literature  $(2.7 \times 10^{-2} \text{ M})^{32}$  and the solubility of CO in THF was estimated from data on the solubility of CO in dioxane  $(4 \times 10^{-4})^{33}$ , which is expected to behave similarly to THF. The concentrations of Cl<sup>-</sup> and any Re complexes were set at  $10^{-4}$  M, as this is the maximum concentration possible under our experimental conditions. 11 Concentration effects were accounted for by relating the law of mass action and the Gibbs free energy of reaction. Thus, for a reaction of the form  $aA \rightleftharpoons bB$ , the effects of concentration outside the standard state of 1 M would be calculated by the formula:  $\Delta G_{\rm sol} = \Delta G_{\rm sol}^0 + RT \ln \left( \frac{[B]^b}{[A]^a} \right)$ . For gaseous reagents and products, the energy associated with compressing the gas from the molar volume of a free gas at STP (22.4 L) was calculated by

the formula: 
$$\Delta H_{\text{Vol}} = -RT \ln \left( \frac{1}{22.4 \left( \frac{L}{\text{mol}} \right) \times [A] \left( \frac{\text{mol}}{L} \right)} \right)$$
, where A is a

Shifts in electron density were investigated via difference densities and Hirshfeld charge analysis: Difference densities were obtained by calculating an oxidized species with the same structure as that of the species of interest and subtracting the electron density of the oxidized species from that of the original state. This is useful for visualizing sites that are likely to undergo electrophilic attack and determining the change in spatial distribution of electron density of species upon reduction. Hirshfeld charges, <sup>34</sup> derived from a spatial based electron density partitioning scheme, were used to gain a more quantitative view of the relative charge distribution. This scheme is less prone to many of the artifacts generated by basis function-based methods such as Mulliken charge analysis. <sup>35</sup>

Free energy of a proton in THF was estimated from the  $pK_a$  value 41.20 of methanol reported in the literature<sup>36</sup> and applying the formulas  $pK_a \times 2.303 \times R \times 298.15 \text{ K} = \Delta G_{\rm THF}$  in conjunction with  $\Delta G_{\rm THF} = G_{\rm THF}({\rm H}^+) + G_{\rm THF}({\rm MeO}^-) - G_{\rm THF}({\rm MeOH})$  to create the expression  $G_{\rm THF}^0({\rm H}^+) = [pK_a \times 2.303 \times R \times 298.15 \text{ K}] - [G_{\rm THF}^0({\rm MeO}^-) - G_{\rm THF}^0({\rm MeOH})]$ . Using calculated values of  $G_{\rm THF}^0({\rm MeO}^-)$  and  $G_{\rm THF}^0({\rm MeOH})$ , we achieved the result of  $G_{\rm THF}^0({\rm H}^+) = -265.4 \text{ kcal/mol}$ . Solving for  $[{\rm H}^+]$  using the literature  $pK_a$  and applying the concentration correction described above yields a  $G_{\rm THF}({\rm H}^+)$  value of -293.8 kcal/mol which was used throughout the study.

Redox potentials were calculated by the formula  $E_{\rm cell} = \frac{-\Delta G_{\rm rm}}{n} + E_{\rm SHE}$  where  $E_{\rm SHE}$  is the mean experimental value of -4.11 V for the absolute value of the SHE as determined by Williams and co-workers.<sup>37,38</sup>

## ■ RESULTS AND DISCUSSION

Electronic Structures of Nanographene Ligand L and Nanographene–Re Complex 1. N-doped nanographenes themselves can be reduced by two electrons. To understand the role of the nanographene ligand L in the reduction of the nanographene–Re complex 1 and CO<sub>2</sub>, we calculated the single-electron frontier orbitals of L and 1, as shown in Figure 1 for HOMO up to (LUMO+4) along with the corresponding orbital energies.

The frontier orbitals of L (upper panel, Figure 1) clearly show partial electron localization over specific regions of the molecule rather than delocalization throughout. For example, the HOMO is mainly located on the hexabenzocoronene moiety of the molecule, and the LUMO on the pyrazine moiety. In the unoccupied orbitals, shown in order of increasing

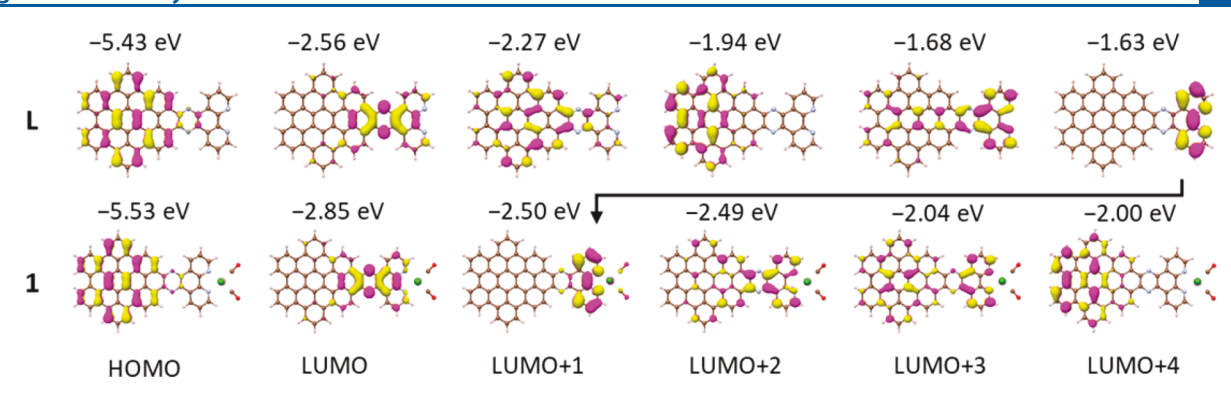


Figure 1. Calculated single-electron molecular orbitals for L (top) and 1 (bottom). All orbitals are rendered with an isovalue of 0.03 au with orbital energies displayed.

energy, contribution from the bipyridine moiety remains insignificant until (LUMO+3) and becomes dominant in (LUMO+4). A similar partial localization of orbitals has been previously reported in dipyridophenazine, a small-molecule analog of L (marked blue in the left panel of Scheme 1), which in metal complexes leads to energetically close states yet with distinct optical properties. 40-42 In L, however, because of the large conjugation size of the hexabenzocoronene moiety, the lowest unoccupied orbitals with significant bipyridine character have much higher energy than the LUMO (at least ~1 eV higher, Figure 1) and thus are not easily electrochemically accessible. In the following discussion, to illustrate the contributions of the specific regions in L for various electrochemical reduction processes, we qualitatively partitioned L into three parts (Scheme 1), and we label them as HBC, Pyraz, and Diim to represent the hexabenzocoronene, pyrazine, and bipyridine (diimine) moieties, respectively.

When L reacts with  $Re^{I}(CO)_{5}Cl$  to form complex 1,<sup>11</sup> all ligand-based orbitals are stabilized due to the polarization by the metal center (Figure 1), with greater stabilization seen on orbitals with significant bipyridine (or Diim) character. As a result, a Diim-dominant orbital reminiscent of (LUMO+4) in L becomes (LUMO+1) of 1, only slightly ( $\sim$ 0.30 eV) above the still Pyraz-dominant LUMO. (LUMO+2) and (LUMO+3) both contain significant Diim-character as well, the former being nearly degenerate with (LUMO+1). These changes in the energy levels lead to drastically different redox properties for 1 compared to L. Overall, 1 is more readily reduced due to the lowered energies of the orbitals. In particular, the orbitals with significant Diim character become readily electrochemically accessible, crucial for CO2 reduction at the metal center as we discuss later. Importantly, a detailed analysis showed that the lowest unoccupied states contain little metal character because of the higher energy of the Re  $d_{x^2-y^2}$  and  $d_{z^2}$  orbitals (vide infra).

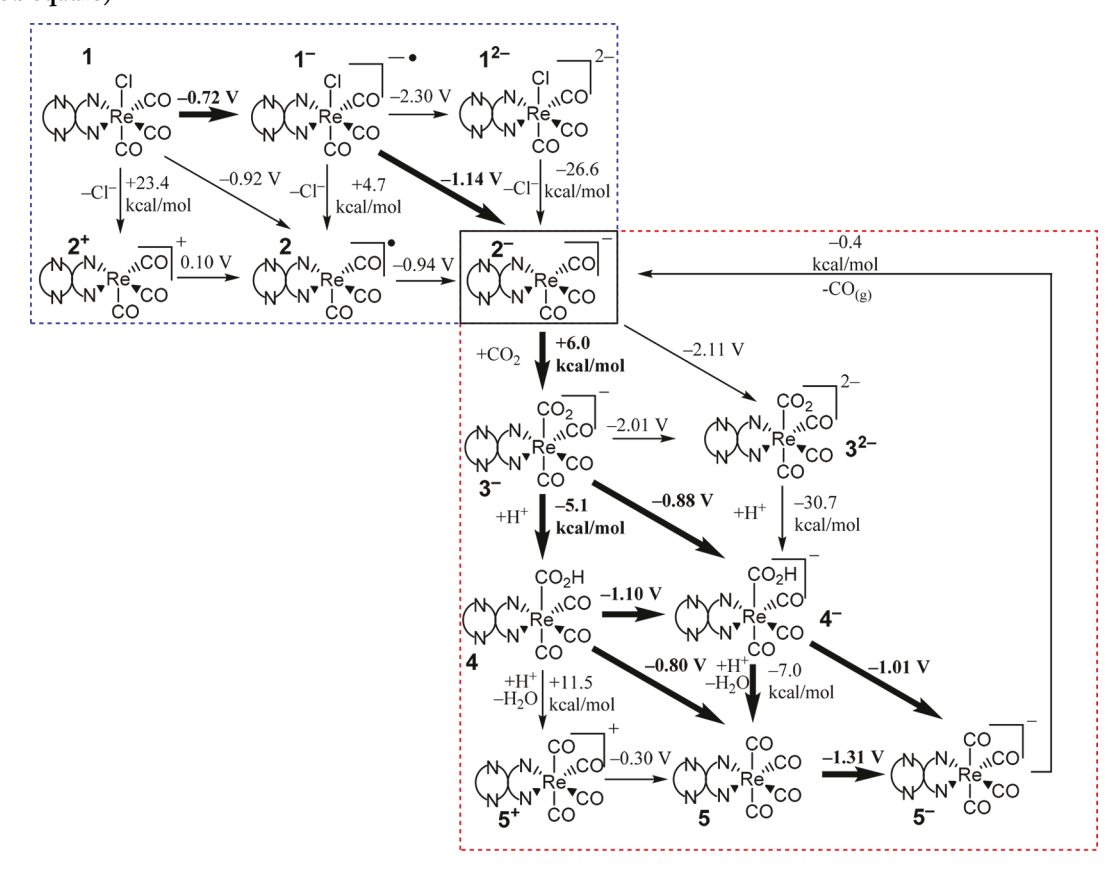
Activation of the Electrocatalyst. Cyclic voltammetry (CV) of 1 in dry THF under inert atmosphere shows two separate one-electron reduction events: a quasi-reversible wave at -0.40 V vs NHE followed by an irreversible reduction with a peak potential at -0.78 V vs NHE. The latter is indicative of a change in molecular geometry associated with electrochemical reduction. This is most likely the dissociation of the axial chloride ligand from the complex based on previous work on the Re(bpy)(CO)<sub>3</sub>Cl system. Indeed, in the presence of CO<sub>2</sub> and a proton source (such as methanol, 5% vol), able to electrocatalyze CO<sub>2</sub> reduction to CO upon the second reduction, indirectly confirming the labilization of Cl<sup>-</sup>. These results are consistent with our calculations outlined in Scheme 2,

in which the energetics of the reduction processes is shown by the reduction potential vs NHE and that of chemical changes shown by the Gibbs free energy. In this study a total of five classes of species are discussed: 2 is produced by the loss of  $Cl^-$  from 1; 3 is generated by binding  $CO_2$  to the resulting five-coordinate Re center; 4 results from the protonation of bound  $CO_2$ ; and 5 is the tetracarbonyl species resulting from the loss of O as water by an addition protonation of metal bound  $CO_2H$ .

According to our calculations, the  $1/1^-$  reduction potential is -0.72 V, which is 0.32 V more negative than the experimental value of -0.40 V. Though the discrepancy is somewhat greater than the more typical deviations in such calculations of  $\pm 0.30$  V, the values are still in fair agreement. 45 The slightly greater discrepancy may be caused by the difference in the interaction between 1 and 1 with the glassy carbon electrode used in the experiments, which will be further studied in the future. In contrast, the calculated  $1^{-}/1^{2-}$  reduction potential is -2.30 V, much too different from the experimental value of -0.78 V to account for the observed second reduction. Instead, alternative and more energetically favorable processes are the reduction of  $1^-$  with concerted loss of Cl<sup>-</sup> at -1.14 V, or a slightly uphill dechlorination step ( $\Delta G^0 = +4.70 \text{ kcal/mol}$ ) followed by a reduction at -0.93 V, both of which lead to the coordinatively unsaturated complex 2-. The potential associated with either of the two pathways is more negative than the experimental value of -0.78 V, though roughly by the same amount as the difference of -0.32 V between the calculated and the experimentally observed potentials for the first reduction. However, the quasi-reversible first reduction experimentally observed indicates dechlorination of 1 is slow on the time scale of the CV measurements. Thus, the concerted reduction and dechlorination of 1 is most likely to be the cause of the experimentally observed second reduction, leading to the coordinatively unsaturated complex 2<sup>-</sup> that performs the subsequent binding and reduction of CO<sub>2</sub>.

Because of the importance of dechlorination for the catalytic activity of 1, we conducted a careful analysis of its driving force. The electronic structures of the reduced species  $\mathbf{1}^-$  and  $\mathbf{1}^{2-}$  were analyzed as well as the electron density changes associated with the reduction processes. Figure 2 shows the calculated electron density difference plots for the reduced species  $\mathbf{1}^-$  and  $\mathbf{1}^{2-}$ . Clearly ligand character is predominant in both cases, though with significantly different spatial distributions, suggesting an open-shell character in  $\mathbf{1}^{2-}$ . The openshell character of the ground state of singlet  $\mathbf{1}^{2-}$  was confirmed by its total spin  $\langle S^2 \rangle$  value of 0.833 (compared to a value of 0.0 for a closed-shell singlet) and found to be 10.0 kcal/mol lower

Scheme 2. Square Scheme Showing Possible Pathways for the Activation of 1 (blue rectangle) and the Binding and Reduction of CO<sub>2</sub> (red square)<sup>a</sup>



<sup>a</sup>The bold arrows represent processes more likely to occur according to comparison between our calculations and the experimental results. The values in the unit of V are calculated reduction potentials in THF relative to the NHE. The values in kcal/mol are calculated Gibbs free energy change of the processes in THF.

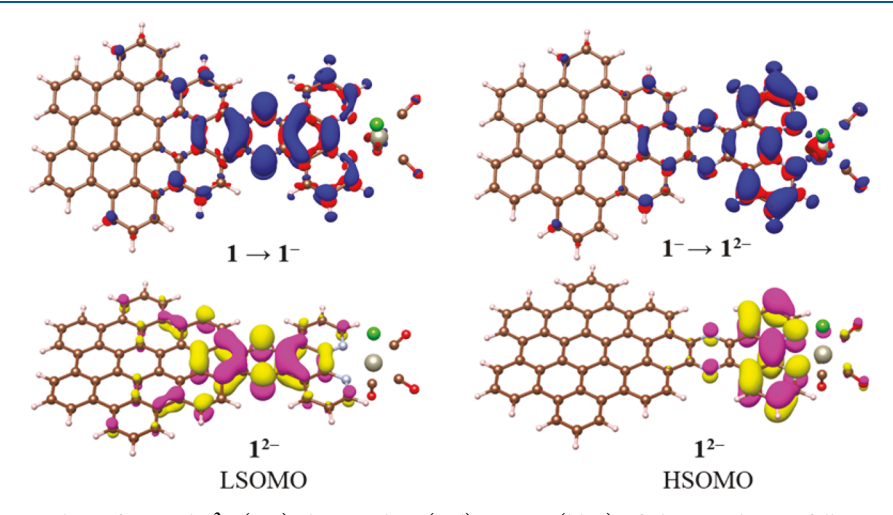


Figure 2. Difference density plots of  $1^-$  and  $1^{2-}$  (top) showing loss (red) or gain (blue) of electron density following the first and the second reduction, respectively. The difference density was obtained relative to the species prior to reduction, that is, the plot for  $1^-$  was obtained with the relaxed geometry of 1, and  $1^{2-}$  with the geometry of  $1^-$ . A detailed description of the charge distribution is in the text (vide infra). Orbital plots (bottom) show the Pyraz-centered LSOMO of  $1^{2-}$  (left) and the Diim-centered HSOMO (right) at isovalues of 0.03 au.

in energy than the triplet state. The highest  $\alpha$  and  $\beta$  orbitals of  $\mathbf{1}^{2-}$  are shown in Figure 2 (lower panel), which have an overlap of 42%, indicating significant spin polarization in the spin unrestricted DFT solution. The higher-energy orbital is centered on the Diim section of  $\mathbf{L}$ , and we designated it as the higher singly occupied molecular orbital (HSOMO). The

lower-energy orbital primarily on Pyraz and HBC is designated the lower singly occupied molecular orbital (LSOMO). The calculated electron density difference plots for the reduced species 1<sup>-</sup> and 1<sup>2-</sup> (Figure 2, upper panel) strongly resemble the LSOMO and the HSOMO, respectively. Most importantly, the electron density change at Re appears negligible in both the

difference density and orbital plots, indicating that neither reduction is metal-centered. This is in strong contrast with previous work on the Re(bpy)(CO)<sub>3</sub>Cl system suggesting that the second reduction should be metal-centered (leading from Re(I) to Re(0)) with consequent labilization of the Cl<sup>-</sup> ligand by occupation of the Re  $d_z^2$  antibonding orbital. An alternative Cl<sup>-</sup> loss pathway was found for Re(bpy)(CO)<sub>3</sub>Cl after the first ligand-centered reduction, though at a slower rate. A7,48

To understand the roles of the various segments in 1 in initiation of the catalysis, we examined the charge redistribution associated with stepwise addition of two electrons to 1. Our analysis shows that the reduction of 1 to 1, a change totaling 1 au of charge, sees L taking on 0.94 au of charge (0.30, 0.27, and 0.37 au for the moieties Diim, Pyraz, and HBC, respectively) and the remaining distributed on Cl-(0.01 au) and the CO ligands (0.05 au). The charge at Re is negligibly altered (0.002 au), consistent with the first reduction being ligand-centered as in the Re(bpy)(CO)<sub>3</sub>Cl case. More importantly, our analysis shows that reduction of 1<sup>-</sup> to 1<sup>2-</sup> is also not a metal-centered reduction and results in no valence change in Re. After the second reduction, the electron density shifts (Figure 2) toward the Diim moiety of L adjacent to Re, but not onto Re itself. Hirshfeld charge analysis comparing 1 with 12- showed the additional portions of charge located on Diim (0.55 au), HBC (0.26 au), the COs (0.10 au), Pyraz (0.05 au), and Cl<sup>-</sup> (0.03 au) with <0.01 au on Re (Table S2). The additional electron density on Cl<sup>-</sup> is due to a small degree of axial ligand character in the HSOMO (vide infra), and the lack of Re character results from the high energy of the Re d<sub>2</sub><sup>2</sup> of  $1^{2-}$  (SI).

The effect of the electrochemical reduction and loss of Cl<sup>-</sup> on the electronic structure of the complex is illustrated with a simplified MO diagram. <sup>49,50</sup> The frontier MOs of  $1^{2-}$  are schematically shown in the left column of Figure 3 and those of  $2^{-}$  in the right, with the orbital compositions qualitatively reflecting the calculated orbitals. For reference we also show MOs with predominant  $d\pi$  components, separated from the higher MOs by a dashed line indicating the existence of other L-centered MOs in between. Of special importance to activation of the catalyst is the LSOMO and the HSOMO of  $1^{2-}$ , neither of which contains appreciable metal character. The LSOMO is largely centered on the Pyraz moiety of L that does not interact strongly with the metal center due to the large distance. The HSOMO consists of  $L\pi^*$  forming an antibonding  $\pi$ -type interaction with an axial  $T_{1u}$ -like ligand orbital.

Loss of the axial Cl<sup>-</sup> in  $1^{2-}$  results in major effects on the electronic structure of the complex. Most importantly, the asymmetric coordination environment along the axial direction leads to the formation of a Re  $d_z^2/p_z$  hybrid orbital. This produces an orbital with the proper symmetry to couple with the  $L\pi^*$  orbital (as in the HSOMO of  $1^{2-}$ ) to form the HOMO of  $2^-$ . The hybrid Re  $d_z^2/p_z$  orbital is still higher in energy than the  $L\pi^*$  orbital, as indicated by the relatively small degree of Re character in the HOMO. The resulting orbital is thus best described as a MO centered on L with some electron donation to the Re  $d_z^2/p_z$  hybrid orbital. Our calculations show that  $2^-$  is a closed-shell species with the triplet state of the same complex less favorable by 5.1 kcal/mol. Attempts to locate a broken symmetry solution only resulted in a closed-shell singlet with an  $\langle S^2 \rangle$  value of 0.0.

Dissociation of Cl $^-$  from  $1^{2-}$  to form  $2^-$  decreases the negative charge on L by 0.76 au, with the charge loss from HBC (0.50 au,), Pyraz (0.26 au), and Diim (<0.01 au) being

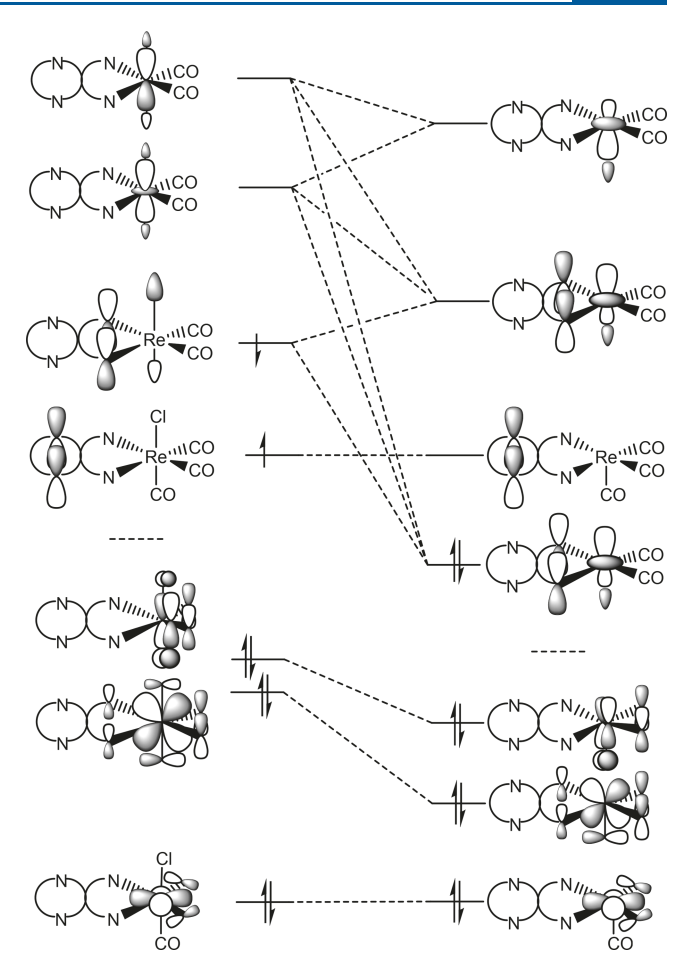


Figure 3. MO diagrams of  $1^{2^-}$  (left) and  $2^-$  (right) showing the consequent polarization and mixing of the Re  $p_z$ , Re  $d_z^2$ , and L  $\pi^*$ . For clarity only the interactions most relevant to the bonding of the metal and the axial ligands are shown, and the L  $\pi^*$  system is represented by a pair of p-like orbitals. The dashed lines in both columns indicate existence of other L-centered MOs with energy in between the frontier MOs and the  $d\pi$ -dominated ones. Orbital compositions were based on calculated orbitals. A selection of these calculated orbitals is available in the SI (Figure S1).

transferred to the CO ligands, Re, and Cl. The departing Cl<sup>-</sup> takes the greatest share of the negative charge (0.53 au) with the three CO ligands sharing 0.15 au and Re gaining 0.09 au. Loss of the Cl<sup>-</sup> ligand lowers the energy of the empty Re  $d_z^2$  MO, increasing the contribution of Re in the HOMO of  $2^-$ . Nevertheless, the HOMO of  $2^-$  is still primarily located on L since the L $\pi^*$  orbitals remain lower than Re  $d_z^2$  even with an open coordination site. As a result, the charge of Re in  $2^-$  is 0.05 au and quite similar to the 0.13 au of Re in 1.

The invariance of the Re oxidation state during the two reductions indicates that  $Cl^-$  lability in  $I^{2-}$  is not a result of a reduced metal center, very different from what is commonly believed for doubly reduced  $Re(bpy)(CO)_3Cl$  complexes. Though the HSOMO of  $I^{2-}$  does show a very small degree of  $d_z^2$  character (Figure 2), it is <2% of the total orbital character. Moreover, the Re–Cl bond length only increases by 0.03 Å upon the second reduction, a change much too small to suggest an antibonding Re–Cl interaction being responsible. In contrast, comparing  $I^{2-}$  to 1, the distance from  $Cl^-$  to the centroid of the Diim moiety increases by 0.12 Å, while the Re–Diim centroid distance remains the same. This suggests that

the negatively charged Cl<sup>-</sup> is repelled by the negatively charged ligand L in 12-. The HSOMO of 12- shows the opposite phase between the coordinating nitrogen atoms in L and Cl with little Re character, indicating a repulsive interaction directly between L and Cl-. The large Diim involvement in the HSOMO of  $1^{2-}$  yields a chemical environment similar to that of Re(bpy)(CO)<sub>3</sub>Cl after the first reduction, since the first electron added to 1 is located on HBC and far from the metal center. It has been demonstrated that loss of an anionic ligand can occur from the mono reduced [Re(bpy)(CO)<sub>3</sub>Cl]<sup>•-</sup> that has little metal radical character, 52 though at a slower rate. This may be a reason for the low turnover frequency in the catalysis of 1 (maximum value being  $3.47 \text{ s}^{-1}$ )<sup>11</sup> and will be further studied. Stabilization of the  $L\pi^*$  by the open Re coordination site results in a closed-shell species upon dissociation of Cl<sup>-</sup>. In comparison to [Re(bpy)(CO)<sub>3</sub>Cl]•-, more electron density is affected in the case of 12- because L is nearly doubly reduced (by 1.80 au). This leads to a greater Coulombic repulsion experienced by Cl- and increases the favorability for the dissociation of Cl<sup>-</sup> for  $1^{2-}$  ( $\Delta G = -26.6$  kcal/mol) compared to  $[\text{Re(bpy)(CO)}_3\text{Cl}]^{\bullet-.53}$ 

The  $\sigma$ -overlap between the Re  $d_z^2/p_z$  hybrid orbital and  $L\pi^*$  in the HOMO of  $2^-$  with a majority of ligand character is consistent with a dative covalent bond between Re and the  $L\pi$  space. Therefore, the overall process to form  $2^-$  can be viewed as a ligand substitution reaction with the  $Cl^-$  ligand being replaced by the  $\pi$  system of L. The driving forces for this displacement are entropic gain by releasing  $Cl^-$  and enthalpic stabilization from the interaction between the Lewis acidic Re  $d_z^2$  and L. The slightly increased electron density at Re suggests that the electron-donating power of the reduced L is greater than  $Cl^-$ , though this change is too small to result in a change in the Re oxidation state. This is consistent with a ligand substitution process as it indicates superior Lewis basicity of the  $L\pi^*$  as compared to  $Cl^-$ , while preserving the oxidation state of ligand and metal.

Activation of  $CO_2$  and Cycling of the Catalyst. Reduction of  $CO_2$  by  $2^-$  proceeds with a nucleophilic attack from Re to the carbon atom in  $CO_2$  to form  $3^-$  with an activation barrier of +13.3 kcal/mol at the transition state  $TS-3^-$  (Figures 4 and S2) and a slight thermodynamic cost

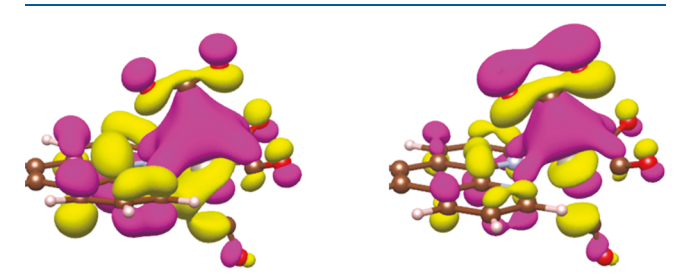


**Figure 4.** Contour plots (isovalue 0.03 au) of the HOMO of TS-3<sup>-</sup>(left) and 3<sup>-</sup> (right) demonstrating increased  $CO_2$  character of the HOMO due to a transfer of electron density from Diim to  $CO_2$  and the nearly invariant density between Re and  $CO_2$ . Overlap between the Diim  $\pi$  system and  $CO_2$  appears to be present in both the species.

 $(\Delta G^0 = +4.4 \text{ kcal/mol}, \text{ red square in Scheme 2})$ . At **TS-3**<sup>-</sup>, the O–C–O angle bends from 180° to 146.9° to decrease C–O antibonding at the metal carboxylate. S4–S6 Distortion of this angle continues along the reaction coordinate to reach 131.6° at the stationary point of CO<sub>2</sub> adduct 3<sup>-</sup>. Disfavoring the binding is the loss of entropy  $(\Delta S \cdot T = +11.2 \text{ kcal/mol})$ 

primarily due to the change in the translational entropy of CO<sub>2</sub> and unfavorable enthalpic contributions due to filled-filled orbital interactions between the  $\pi$  orbitals of CO<sub>2</sub> and the d $\pi$ orbitals of Re (Figures S3 and S4). In contrast, 3<sup>-</sup> is stabilized largely by solvation. As solvation free energy is more favorable as charge density increases, concentration of the negative charge at the oxygen atoms leads to a greater solvation stabilization for 3<sup>-</sup> than for 2<sup>-</sup>. Indeed, the combined ZPE and electronic energy is 5.3 kcal/mol higher on the product side than it is at the transition state, but this is compensated by -13.8 kcal/mol of solvation stabilization in  $3^-$  (Table S1). It appears that the transition state is close to the point where enough electron density is localized on the oxygen atoms of CO<sub>2</sub> that the solvation term begins to dominate the energetics, leading to further charge transfer from L to CO<sub>2</sub> and formation of 3<sup>-</sup>. It is worth noting that computational studies on Re(bpy) (CO)<sub>3</sub>Cl have also shown that CO<sub>2</sub> binding is possible only when there is stabilization of charge on the oxygen atoms with either solvation corrections or metal cations.<sup>20</sup>

Initially higher than the  $L\pi^*$  orbital, the energy of the  $CO_2$   $\pi^*$  orbital is decreased significantly by interaction with the Re center, resulting in transfer of electrons from L to  $CO_2$  which is driven to completion by solvation. Throughout this process there is little change to the electron density at Re. The invariant Re oxidation state indicates that this system acts as a mediator in the reaction: facilitating transfer of two electrons, while simultaneously stabilizing the resulting dianionic  $CO_2$  species as a Lewis acid. It is therefore cogent to characterize Re as a conduit in this transaction to facilitate charge transfer between two termini while itself maintaining a steady degree of electron density. This can be visualized by comparing the isodensity plots of the HOMOs of TS-3<sup>-</sup> and 3<sup>-</sup> which demonstrate a transfer of electron density from L to  $CO_2$  with nearly constant electron density at Re (Figure 4).

Despite the slightly unfavored  $CO_2$  binding, at the applied potential (-1.14 V),  $3^-$  can be readily depleted, shifting the equilibrium to favor binding of  $CO_2$ . According to our calculations, depletion of  $3^-$  can proceed through two pathways (Scheme 2). It can undergo a highly favored protonation (4), followed by or concerted with a reduction ( $4^-$ ). In 4, L is more electron deficient by 0.04 au than that in 1, enabling further reduction of 4 at the applied potential. Similarly, under the applied potential, both 4 and  $4^-$  can undergo further protonation at oxygen and reduction/dehydration to produce  $5^-$  and, by eliminating a CO ligand, to regenerate  $2^-$  (Scheme 2) for more catalytic cycles. Similar to the results previously shown for Re(bpy)(CO)<sub>3</sub>Cl and Mn(bpy)(CO)<sub>3</sub>Br, the dehydration may occur through a "protonation-first" or a "reduction-first" pathway.  $^{17,57,58}$ 

The lability of CO from  $5^-$  is similar to the loss of Cl<sup>-</sup> from  $1^{2^-}$  in that both events involve replacing a ligand with the basic  $L\pi^*$  orbital and gaining entropy by releasing a ligand molecule. Even though CO binds more strongly to Re, the entropy gain in losing the CO is sufficient to override the binding enthalpy, making CO dissociation favorable by -0.4 kcal/mol under 1 atm of CO gas, and even more favorable under a lower partial pressure of CO in experiments ( $\sim 10^{-3}$  atm). Further, CO dissociation is kinetically favored. Relaxed surface scans show that elongating the Re–CO distance has no visible barrier on the potential energy surface, perhaps due to interactions between the CO  $\pi^*$  and  $L\pi^*$  systems as the Re–CO distance increases (Figure SS). Thus, regeneration of  $2^-$  from  $5^-$  by releasing CO is expected to proceed rapidly at the applied potential.

Again, the Re oxidation state is nearly constant, with a Hirshfeld charge of 0.14 au calculated for 12-, 0.05 au for both 2 and TS-3, 0.07 au upon formation of the CO<sub>2</sub> adduct 3, and 0.10 au upon protonation to 4. In contrast, for the same reactions, L is oxidized from -1.18 au in  $1^{2-}$  to -0.42 au in  $2^{-}$ to -0.16 au in TS-3, 0.22 au when CO<sub>2</sub> is bound in 3, and finally to 0.59 au upon protonation to 4, with a total variation of 1.77 au in contrast to the 0.09 au at Re in these reactions (Table S2). The lack of charge variation at Re in the transition state of CO<sub>2</sub> binding is particularly striking. Even at the energy maximum, L appears to transfer charge directly to CO2 without increasing the electron density at Re. MO diagrams (Figure 4) support this picture as well, showing very little change in the Re character during and after CO2 binding, but a drastic increase in CO2 character and decrease in Diim character in the HOMO.

#### SUMMARY AND CONCLUDING REMARKS

Here we elucidated the mechanism for electrocatalytic  $CO_2$  reduction by the nanographene complex 1 with DFT calculations and Hirshfeld charge analysis. Our calculations revealed the driving force for dissociation of  $Cl^-$  upon two-electron reduction of 1 to form the catalytically active  $2^-$ . Addition of  $CO_2$  to this species is followed by abstraction of oxygen by protonation and concerted or stepwise two electron reduction to generate water and the tetracarbonyl species  $5^-$ .  $2^-$  is regenerated after release of an axial CO, enabling further catalytic cycles.

One of the most unexpected observations in this study is the invariance of the oxidation state of Re with Hirshfeld charges varying no more than 0.10 au (being the highest in 1, 0.15 au, and the lowest in  $2^-$ , 0.05 au). Even though reduction of CO<sub>2</sub> occurs at the metal center the overall catalytic reaction is better described by transfer of electron density from a two-electron reduced ligand L to CO2. This is evident starting from the labilization of chloride to binding and subsequent reduction of CO<sub>2</sub>. Upon binding CO<sub>2</sub> the Diim, HBC, and Pyraz moieties contribute -0.55, -0.06, and -0.04 au of charge, respectively, to the substrate. Re and the COs only contribute -0.02 au and -0.10 au in total leading to a total charge of -0.77 au on  $CO_2$ . At TS-3<sup>-</sup>, the electron loss at L and the gain at the CO<sub>2</sub> is equal so that the oxidation state of Re does not change significantly. Thus, it is clear that the role of the metal is as a conduit to facilitate electron transfer rather than a reductant or oxidant. This perhaps should not be surprising, considering the relative energies of the L $\pi^*$  orbitals and the substrate. For Re to change its oxidation state in this reaction, the Re  $d_z^2$  level would have to be even lower in energy than the  $L\pi^*$  orbitals. Because L has a much larger conjugated  $\pi$  system and contains several nitrogen heteroatoms, the  $L\pi^*$  orbital energy is already lower than the CO<sub>2</sub>  $\pi^*$ . Thus, under the reaction conditions, the stabilization due to solvation is the primary factor driving the electron transfer from L to CO<sub>2</sub>. If the orbital energy of the metal is low enough for reduction to occur there, then the electron transfer would be energetically much less favorable and binding of CO2 would not occur. Rather, the role of Re is mostly that of a Lewis acid which acts to stabilize negatively charged ligands in its coordination sphere through covalent overlap with the Re  $d_z^2$ . This stands in contrast to experimental and theoretical work on Re(bpy)(CO)<sub>3</sub> which has been explicit in identifying the metal as redox active. 53,59

It is well understood that d<sup>6</sup> metal electron configurations and octahedral coordination environments are particularly

stable for metal complexes, and it appears that the metal center for this system conforms well to that maxim. All the accessible states are consistent with a Re(I) oxidation state and a sixcoordinate environment. This may include the approximately square pyramidal 3<sup>-</sup> if we consider the covalency of the Re- $L\pi^*$  interaction to be a dative bond, an assertion supported by the relatively small degree of metal character in its HOMO. This is possible because the surrounding ligands are much easier to reduce and oxidize than the metal center throughout the catalytic cycle. However, this does not mean that the metal center is unimportant. Its role appears different from what we would have anticipated based on previous studies on similar complexes with smaller diimine ligands. Based on our studies, clearly Re is crucial for the polarization of L in 1, suppressing the energy of unoccupied orbitals, especially those with significant Diim characters to make them electrochemically accessible (Figure 1). This makes it possible to electrochemically produce a species (1<sup>2-</sup>) with significant Diim character in its HSOMO to drive labilization of the axial halide and formation of 2-. Labilization of the halide further stabilizes the Diimdominant orbitals, resulting in the HOMO, located primarily on Diim, to facilitate binding and reduction of CO<sub>2</sub>. Thus, another role of Re appears to be in stabilization of involved orbitals through its Lewis acidity rather than participation as a redox active component. Other more earth-abundant metals may be able to play the same roles as well and are being investigated as potential substitutes for Re in the nanographene complexes for electrocatalytic and photocatalytic CO<sub>2</sub> reduction.

#### ASSOCIATED CONTENT

## **S** Supporting Information

The Supporting Information is available free of charge on the ACS Publications website at DOI: 10.1021/acs.inorgchem.8b01092.

Details of calculated MOs and analysis, reaction pathways, detailed charge analysis, and atomic coordinates of key species (PDF)

### AUTHOR INFORMATION

## **Corresponding Authors**

\*E-mail: kraghava@indiana.edu. \*E-mail: li23@indiana.edu.

ORCID (

Krishnan Raghavachari: 0000-0003-3275-1426

Liang-shi Li: 0000-0001-7566-8492

Notes

The authors declare no competing financial interest.

## ACKNOWLEDGMENTS

We acknowledge the financial support of the National Science Foundation (grants CHE-1665427 KR and CBET-1610712 to L.L.). This research was supported in part by Lilly Endowment, Inc., through its support for the Indiana University Pervasive Technology Institute, and in part by the Indiana METACyt Initiative.

### REFERENCES

(1) Whipple, D. T.; Kenis, P. J. A. Prospects of  $\mathrm{CO}_2$  Utilization via Direct Heterogeneous Electrochemical Reduction. *J. Phys. Chem. Lett.* **2010**, *1* (24), 3451–3458.

(2) Morris, A. J.; Meyer, G. J.; Fujita, E. Molecular Approaches to the Photocatalytic Reduction of Carbon Dioxide for Solar Fuels. *Acc. Chem. Res.* **2009**, 42 (12), 1983–1994.

(3) Benson, E. E.; Kubiak, C. P.; Sathrum, A. J.; Smieja, J. M. Electrocatalytic and homogeneous approaches to conversion of CO<sub>2</sub> to liquid fuels. *Chem. Soc. Rev.* **2009**, 38 (1), 89–99.

- (4) Kumar, B.; Llorente, M.; Froehlich, J.; Dang, T.; Sathrum, A.; Kubiak, C. P. Photochemical and Photoelectrochemical Reduction of CO<sub>2</sub>. *Annu. Rev. Phys. Chem.* **2012**, *63* (1), 541–569.
- (5) Goeppert, A.; Czaun, M.; Jones, J.-P.; Surya Prakash, G. K.; Olah, G. A. Recycling of carbon dioxide to methanol and derived products closing the loop. *Chem. Soc. Rev.* **2014**, *43* (23), 7995–8048
- (6) White, J. L.; Baruch, M. F.; Pander, J. E.; Hu, Y.; Fortmeyer, I. C.; Park, J. E.; Zhang, T.; Liao, K.; Gu, J.; Yan, Y.; Shaw, T. W.; Abelev, E.; Bocarsly, A. B. Light-Driven Heterogeneous Reduction of Carbon Dioxide: Photocatalysts and Photoelectrodes. *Chem. Rev.* 2015, 115 (23), 12888–12935.
- (7) Appel, A. M.; Bercaw, J. E.; Bocarsly, A. B.; Dobbek, H.; DuBois, D. L.; Dupuis, M.; Ferry, J. G.; Fujita, E.; Hille, R.; Kenis, P. J. A.; Kerfeld, C. A.; Morris, R. H.; Peden, C. H. F.; Portis, A. R.; Ragsdale, S. W.; Rauchfuss, T. B.; Reek, J. N. H.; Seefeldt, L. C.; Thauer, R. K.; Waldrop, G. L. Frontiers, Opportunities, and Challenges in Biochemical and Chemical Catalysis of CO<sub>2</sub> Fixation. *Chem. Rev.* **2013**, *113* (8), 6621–6658.
- (8) Francke, R.; Schille, B.; Roemelt, M. Homogeneously Catalyzed Electroreduction of Carbon Dioxide—Methods, Mechanisms, and Catalysts. *Chem. Rev.* **2018**, *118* (9), 4631–4701.
- (9) Costentin, C.; Robert, M.; Saveant, J.-M. Catalysis of the electrochemical reduction of carbon dioxide. *Chem. Soc. Rev.* **2013**, 42 (6), 2423–2436.
- (10) Oh, S.; Gallagher, J. R.; Miller, J. T.; Surendranath, Y. Graphite-Conjugated Rhenium Catalysts for Carbon Dioxide Reduction. *J. Am. Chem. Soc.* **2016**, *138* (6), 1820–1823.
- (11) Qiao, X.; Li, Q.; Schaugaard, R. N.; Noffke, B. W.; Liu, Y.; Li, D.; Liu, L.; Raghavachari, K.; Li, L.-s. Well-Defined Nanographene—Rhenium Complex as an Efficient Electrocatalyst and Photocatalyst for Selective CO<sub>2</sub> Reduction. *J. Am. Chem. Soc.* **2017**, *139* (11), 3934–3937.
- (12) Neese, F. The ORCA program system. Wiley Interdisciplinary Reviews: Computational Molecular Science 2012, 2 (1), 73–78.
- (13) Vosko, S. H.; Wilk, L.; Nusair, M. Accurate spin-dependent electron liquid correlation energies for local spin density calculations: a critical analysis. *Can. J. Phys.* **1980**, *58* (8), 1200–1211.
- (14) Lee, C.; Yang, W.; Parr, R. G. Development of the Colle-Salvetti correlation-energy formula into a functional of the electron density. *Phys. Rev. B: Condens. Matter Mater. Phys.* **1988**, 37 (2), 785–789
- (15) Becke, A. D. Density-functional exchange-energy approximation with correct asymptotic behavior. *Phys. Rev. A: At., Mol., Opt. Phys.* **1988**, 38 (6), 3098–3100.
- (16) Becke, A. D. A new mixing of Hartree-Fock and local density-functional theories. *J. Chem. Phys.* **1993**, 98 (2), 1372–1377.
- (17) Riplinger, C.; Sampson, M. D.; Ritzmann, A. M.; Kubiak, C. P.; Carter, E. A. Mechanistic Contrasts between Manganese and Rhenium Bipyridine Electrocatalysts for the Reduction of Carbon Dioxide. *J. Am. Chem. Soc.* **2014**, *136* (46), 16285–16298.
- (18) Keith, J. A.; Grice, K. A.; Kubiak, C. P.; Carter, E. A. Elucidation of the Selectivity of Proton-Dependent Electrocatalytic CO2 Reduction by fac-Re(bpy)(CO)3Cl. *J. Am. Chem. Soc.* **2013**, *135* (42), 15823–15829.
- (19) Grimme, S.; Antony, J.; Ehrlich, S.; Krieg, H. A consistent and accurate ab initio parametrization of density functional dispersion correction (DFT-D) for the 94 elements H-Pu. *J. Chem. Phys.* **2010**, 132 (15), 154104.
- (20) Johnson, E. R.; Becke, A. D. A post-Hartree–Fock model of intermolecular interactions. *J. Chem. Phys.* **2005**, *123* (2), 024101.
- (21) Becke, A. D.; Johnson, E. R. A density-functional model of the dispersion interaction. *J. Chem. Phys.* **2005**, *123* (15), 154101.
- (22) Johnson, E. R.; Becke, A. D. A post-Hartree-Fock model of intermolecular interactions: Inclusion of higher-order corrections. *J. Chem. Phys.* **2006**, *124* (17), 174104.

- (23) Schäfer, A.; Horn, H.; Ahlrichs, R. Fully optimized contracted Gaussian basis sets for atoms Li to Kr. *J. Chem. Phys.* **1992**, *97* (4), 2571–2577.
- (24) Andrae, D.; Häußermann, U.; Dolg, M.; Stoll, H.; Preuß, H. Energy-adjusted initio pseudopotentials for the second and third row transition elements: Molecular test for  $M_2$  (M = Ag, Au) and MH (M = Ru, Os). Theor. Chem. Acta 1991, 78 (4), 247–266.
- (25) Klamt, A.; Schuurmann, G. COSMO: a new approach to dielectric screening in solvents with explicit expressions for the screening energy and its gradient. *J. Chem. Soc., Perkin Trans.* 2 **1993**, No. 5, 799–805.
- (26) Smieja, J. M.; Benson, E. E.; Kumar, B.; Grice, K. A.; Seu, C. S.; Miller, A. J. M.; Mayer, J. M.; Kubiak, C. P. Kinetic and structural studies, origins of selectivity, and interfacial charge transfer in the artificial photosynthesis of CO. *Proc. Natl. Acad. Sci. U. S. A.* **2012**, 109 (39), 15646–15650.
- (27) Schäfer, A.; Huber, C.; Ahlrichs, R. Fully optimized contracted Gaussian basis sets of triple zeta valence quality for atoms Li to Kr. *J. Chem. Phys.* **1994**, *100* (8), 5829–5835.
- (28) Weigend, F.; Ahlrichs, R. Balanced basis sets of split valence, triple zeta valence and quadruple zeta valence quality for H to Rn: Design and assessment of accuracy. *Phys. Chem. Chem. Phys.* **2005**, 7 (18), 3297–3305.
- (29) Papajak, E.; Leverentz, H. R.; Zheng, J.; Truhlar, D. G. Efficient Diffuse Basis Sets: cc-pVxZ+ and maug-cc-pVxZ. J. Chem. Theory Comput. 2009, 5 (5), 1197–1202.
- (30) Papajak, E.; Truhlar, D. G. Efficient Diffuse Basis Sets for Density Functional Theory. *J. Chem. Theory Comput.* **2010**, 6 (3), 597–601.
- (31) McQuarrie, D. A. Statistical Mechanics; University Science Books: Sausalito, CA, 2000.
- (32) Fogg, P. G. T. IUPAC Solubility Data Series: Carbon Dioxide in Non-Aqueous Solvents at Pressures Less Than 200 kPa; Pergamon Press Ltd.: Oxford, 1992; Vol. 50, p 202.
- (33) Veleckis, E.; Hacker, D. S. Solubility of carbon monoxide in 1,4-dioxane. *J. Chem. Eng. Data* **1984**, 29 (1), 36–39.
- (34) Hirshfeld, F. L. Bonded-atom fragments for describing molecular charge densities. *Theor. Chim. Acta* 1977, 44 (2), 129–138.
- (35) Mulliken, R. S. Electronic Population Analysis on LCAO-MO Molecular Wave Functions. I. J. Chem. Phys. 1955, 23 (10), 1833–1840
- (36) Ding, F.; Smith, J. M.; Wang, H. First-Principles Calculation of pKa Values for Organic Acids in Nonaqueous Solution. *J. Org. Chem.* **2009**, 74 (7), 2679–2691.
- (37) Donald, W. A.; Leib, R. D.; O'Brien, J. T.; Bush, M. F.; Williams, E. R. Absolute Standard Hydrogen Electrode Potential Measured by Reduction of Aqueous Nanodrops in the Gas Phase. *J. Am. Chem. Soc.* **2008**, *130* (11), 3371–3381.
- (38) Donald, W. A.; Leib, R. D.; Demireva, M.; O'Brien, J. T.; Prell, J. S.; Williams, E. R. Directly Relating Reduction Energies of Gaseous  $\mathrm{Eu}(\mathrm{H_2O})_n^{3+}$ , n=55-140, to Aqueous Solution: The Absolute SHE Potential and Real Proton Solvation Energy. *J. Am. Chem. Soc.* **2009**, 131 (37), 13328–13337.
- (39) Li, Q.; Noffke, B.; Wang, Y.; Menezes, B.; Peters, D. G.; Raghavachari, K.; Li, L.-S. Electrocatalytic Oxygen Activation by Carbanion Intermediates of Nitrogen-Doped Graphitic Carbon. *J. Am. Chem. Soc.* **2014**, *136*, 3358–3361.
- (40) Friedman, A. E.; Chambron, J. C.; Sauvage, J. P.; Turro, N. J.; Barton, J. K. A Molecular Light Switch for DNA: Ru(bpy)<sub>2</sub>(dppz)<sup>2+</sup>. *J. Am. Chem. Soc.* **1990**, *112*, 4960–4962.
- (41) Brennaman, M. K.; Alstrum-Acevedo, J. H.; Fleming, C. N.; Jang, P.; Meyer, T. J.; Papanikolas, J. M. Turning the [Ru(bpy)-2dppz]2+ Light-Switch On and Off with Temperature. *J. Am. Chem. Soc.* **2002**, *124*, 15094–15098.
- (42) Lundin, N. J.; Walsh, P. J.; Howell, S. L.; McGarvey, J. J.; Blackman, A. G.; Gordon, K. C. Complexes of Functionalized Dipyrido[3,2-a:2',3'-c]-phenazine: A Synthetic, Spectroscopic, Structural, and Density Functional Theory Study. *Inorg. Chem.* **2005**, *44* (10), 3551–3560.

(43) Bard, A. J.; Faulkner, L. R.; Leddy, J.; Zoski, C. G. Electrochemical Methods: Fundamentals and Applications; Wiley: New York, 1980; Vol. 2.

- (44) Keith, J. A.; Carter, E. A. Quantum Chemical Benchmarking, Validation, and Prediction of Acidity Constants for Substituted Pyridinium Ions and Pyridinyl Radicals. *J. Chem. Theory Comput.* **2012**, 8 (9), 3187–3206.
- (45) Noffke, B. W.; Li, Q.; Raghavachari, K.; Li, L.-S. A Model for the pH-Dependent Selectivity of the Oxygen Reduction Reaction Electrocatalyzed by N-Doped Graphitic Carbon. *J. Am. Chem. Soc.* **2016**, *138*, 13923–13929.
- (46) Sullivan, B. P.; Bolinger, C. M.; Conrad, D.; Vining, W. J.; Meyer, T. J. One- and two-electron pathways in the electrocatalytic reduction of  $CO_2$  by fac-Re(bpy)( $CO)_3$ Cl (bpy = 2,2'-bipyridine). *J. Chem. Soc., Chem. Commun.* **1985**, 20, 1414–1416.
- (47) Klein, A.; Vogler, C.; Kaim, W. The d in 18 + d Electron Complexes: Importance of the Metal/Ligand Interface for the Substitutional Reactivity of "Re(0)" Complexes (a-diimine<sup>-</sup>)-Re<sup>I</sup>(CO)<sub>3</sub>(X). Organometallics 1996, 15, 236–244.
- (48) Stor, G. J.; Hartl, F.; van Outersterp, J. W. M.; Stufkens, D. J. Spectroelectrochemical (IR, UV/Vis) Determination of the Reduction Pathways for a Series of [Re(CO)<sub>3</sub>(a-diimine)L']O(/L' = Halide, Otf<sup>-</sup>, THF, MeCN, n-PrCN, PPh<sub>3</sub>, P(OMe)<sub>3</sub>) Complexes. *Organometallics* 1995, *14*, 1115–1131.
- (49) Jean, Y. Molecular Orbitals of Transition Metal Complexes; Oxford University Press: Oxford, 2003.
- (50) Albright, T. A.; Burdett, J. K.; Whangbo, M.-H. Transition Metal Complexes: A Starting Point at the Octahedron. In *Orbital Interactions in Chemistry*; John Wiley & Sons, Inc.: Hoboken, NJ, 2013; pp 401–435.
- (51) Albright, T. A.; Burdett, J. K.; Whangbo, M.-H. Five Coordination. In *Orbital Interactions in Chemistry*; John Wiley & Sons, Inc.: Hoboken, NJ, 2013; pp 465–502.
- (52) Scheiring, T.; Klein, A.; Kaim, W. EPR study of paramagnetic rhenium(I) complexes (bpy)Re(CO)<sub>3</sub>X relevant to the mechanism of electrocatalytic CO<sub>2</sub> reduction. *J. Chem. Soc., Perkin Trans.* 2 **1997**, No. 12, 2569–2572.
- (53) Keith, J. A.; Grice, K. A.; Kubiak, C. P.; Carter, E. A. Elucidation of the Selectivity of Proton-Dependent Electrocatalytic CO<sub>2</sub> Reduction by fac-Re(bpy)(CO)<sub>3</sub>Cl. *J. Am. Chem. Soc.* **2013**, *135* (42), 15823–15829.
- (54) Walsh, A. D. 466. The electronic orbitals, shapes, and spectra of polyatomic molecules. Part I. AH2 molecules. *J. Chem. Soc.* **1953**, *0*, 2260–2266.
- (55) Walsh, A. D. 467. The electronic orbitals, shapes, and spectra of polyatomic molecules. Part II. Non-hydride AB2 and BAC molecules. *J. Chem. Soc.* **1953**, *0*, 2266–2288.
- (56) Freund, H. J.; Roberts, M. W. Surface chemistry of carbon dioxide. Surf. Sci. Rep. 1996, 25 (8), 225–273.
- (57) Riplinger, C.; Carter, E. A. Influence of Weak Brønsted Acids on Electrocatalytic CO2 Reduction by Manganese and Rhenium Bipyridine Catalysts. ACS Catal. 2015, 5 (2), 900–908.
- (58) Ngo, K. T.; McKinnon, M.; Mahanti, B.; Narayanan, R.; Grills, D. C.; Ertem, M. Z.; Rochford, J. Turning on the Protonation-First Pathway for Electrocatalytic CO2 Reduction by Manganese Bipyridyl Tricarbonyl Complexes. J. Am. Chem. Soc. 2017, 139 (7), 2604–2618.
- (59) Benson, E. E.; Sampson, M. D.; et al. The Electronic States of Rhenium Bipyridyl Electrocatalysts for CO2 Reduction as Revealed by X-ray Absorption Spectroscopy and Computational Quantum Chemistry. *Angew. Chem., Int. Ed.* **2013**, 52 (18), 4841–4844.